AIP | Journal of Applied Physics

Bias-enhanced nucleation and growth processes for improving the electron field emission properties of diamond films

Kuang-Yau Teng, Huang-Chin Chen, Gaung-Chin Tzeng, Chen-Yau Tang, Hsiu-Fung Cheng, and I-Nan Lin

Citation: Journal of Applied Physics **111**, 053701 (2012); doi: 10.1063/1.3687918
View online: http://dx.doi.org/10.1063/1.3687918
View Table of Contents: http://scitation.aip.org/content/aip/journal/jap/111/5?ver=pdfcov
Published by the AIP Publishing

Bias-enhanced nucleation and growth processes for improving the electron field emission properties of diamond films

Kuang-Yau Teng,[1] Huang-Chin Chen,[1] Gaung-Chin Tzeng,[1] Chen-Yau Tang,[1] Hsiu-Fung Cheng,[2] and I-Nan Lin[1,a)]
[1]*Department of Physics, Tamkang University, Tamsui 251, Taiwan*
[2]*Department of Physics, National Taiwan Normal University, Taipei 106, Taiwan*

(Received 25 November 2011; accepted 28 January 2012; published online 1 March 2012)

The evolution of diamond films in bias-enhanced-nucleation (BEN) and bias-enhanced-growth (BEG) processes was systematically investigated. While the BEN process can efficiently form diamond nuclei on the Si substrates, BEG with large enough applied field (> –400 V) and for sufficiently long periods (>60 min) was needed to develop proper granular structure for the diamond films so as to enhance the electron field emission (EFE) properties of the films. For the films BEG under −400 V for 60 min (after BEN for 10 min), the EFE process can be turned on at a field as small as 3.6 V/μm, attaining a EFE current density as large as 325 μA/cm^2 at an applied field of 15 V/μm. Such an EFE behavior is even better than that of the ultrananocrystalline diamond films grown in CH_4/Ar plasma. Transmission electron microscopic examination reveals that the prime factor enhancing the EFE properties of these films is the induction of the nano-graphite filaments along the thickness of the films that facilitates the transport of electrons through the films. © *2012 American Institute of Physics*. [http://dx.doi.org/10.1063/1.3687918]

I. INTRODUCTION

Diamond films possess many marvelous physical and chemical properties[1–3] and were the focus of intensive research since the successful synthesis of the diamond in low pressure and low temperature chemical vapor deposition (CVD) process.[4] The negative electron affinity (NEA)[5] characteristic of diamond films observed for re-constructed (100) surface was thought to be of great potential for applications as electron field emitters.[6,7] However, a good diamond electron field emitter requires, besides the NEA surface, sufficient supply of electrons from the back electrode materials and effective transport of electrons through the diamond. The diamond films, which were grown in CH_4/H_2 plasma, usually contain large grains (microcrystalline diamond (MCD)) with a large electron bandgap (5.1 eV). Such a large electronic bandgap hinders the electron field emission (EFE) behavior of the materials due to lack of electrons required for field emission. Doping the MCD films with boron or nitrogen species provides abundant intraband energy levels that have been observed to markedly enhance the EFE of the materials.[8–12] However, the EFE properties for these diamonds are still not satisfactory, owing to the fact that the boron species actually are accepters, whereas the nitrogen species form deep donors.[13,14] The boron and nitrogen doping do not supply sufficient electrons for the field emission purpose. Ultrananocrystalline diamond (UNCD) films contain nano-sized grains with grain boundaries of considerable thickness, which contain sp^2-bonds and possess good conductivity.[15] The transport of electrons through the UNCD films is markedly better than that through the MCD films. Therefore, the UNCD films possess superior EFE properties to the MCD films.[16,17] However, the conductivity of conventional UNCD films grown in CH_4/Ar plasma is still large, ~ hundreds of (ohm cm)$^{-1}$ which is significantly smaller than those of the other nano-carbon materials, such as carbon nanotubes,[18,19] carbon nano-flakes,[20–22] etc. The UNCD films still exhibit markedly inferior EFE properties as compared with the nano-carbon materials. Previously, Chen *et al.*[23] observed that the application of bias voltage in the CH_4/H_2 plasma, microwave plasma-enhanced CVD process not only facilitated the growth of diamond, but also efficiently reduced the size of the grains, resulting in diamond films with nano-sized granular structure. Such a nanocrystalline microstructure is expected to enhance the EFE properties of the films, but the EFE behavior of the bias-enhanced grown diamond films have not been reported.

In this paper, we used the bias-enhanced nucleation and bias-enhanced growth (BEN-BEG) in microwave plasma—enhanced CVD (MPE-CVD) process to alter the granular structure of the diamond films. We obtained diamond films with nano-sized grains that exhibited enhanced EFE properties. The evolution in granular structure of the diamond films with the applied bias was detailedly examined using transmission electron microscopy (TEM). The possible mechanism that enhanced EFE properties for the films was discussed.

II. EXPERIMENTALS

The diamond films were grown on p-type silicon substrate by a modified MPE-CVD process. The substrates were first thoroughly cleaned by rinsing the Si wafer sequentially in water-diluted hydrogen peroxide/ammonium hydroxide and hydrogen peroxide/hydrochloric acid solution, followed by washing in deionized water. The diamond films were grown in CH_4/H_2 = 9/91 sccm plasma and excited by a 1400 W (2.45 GHz) microwave with a 40 Torr total pressure.

a)Author to whom correspondence should be addressed. Electronic mail: inanlin@mail.tku.edu.tw.

A negative bias voltage (−400 V) was applied to the Si substrates during the nucleation stage (BEN, 10 min), and 0 to −500 V bias voltage was applied in the growth period (BEG, 60 min). The morphology and structure of the films were investigated using scanning electron microscopy (SEM, Joel JSM-6500 F) and Raman spectroscopy (Renishaw inVia Raman microscopes). The detail microstructure was examined using transmission electron microscopy (TEM, Joel 2100). The EFE properties of diamond films were measured using a parallel plate setup, in which the cathode-to-anode distance was set by a fixed spacer (125 μm) and the current-voltage (I-V) characteristics were acquired by Keithley 2410 in a 10^{-6} Torr environment. The EFE properties were analyzed by the Fowler-Nordheim (F-N) model,[24] and the turn-on field was designated as the interception of the straight lines extrapolated from the high-field and low-field segments of F-N plots.

III. RESULTS AND DISCUSSION

A. Plasma and diamond characteristics

The capability of *in situ* monitoring the characteristics of plasma is of critical importance in the development of the MPE-CVD process for optimizing the characteristics of the diamond films. In our reactor, the plasma was confined in a cylindrical quartz around 20 cm in diameter (10 cm in height) that allowed the fabrication of narrow rectangular slits on the wall of the metallic microwave applicators for monitoring the plasma using optical emission spectroscopy (OES). The plasma ball is usually in a form of spherical or oval geometry when there is no bias voltage applied to the substrates. Figure 1(a) shows the photograph of the plasma viewed through the slits of the microwave applicator. The color of the plasma changed from light blue in H_2 plasma (photograph I) to purplish-blue in CH_4(9%)/H_2 plasma (photograph II), which is ascribed to the presence of carbonaceous (or hydrocarbon) species in the plasma. Once the negative bias voltage was applied to the Si substrates, the color of the plasma became purplish-pink (photographs III-VII), which presumably resulted from the depletion of the positively charged species (H^+, CH^+, CH_3^+,…) from the center of the H_2 plasma. In the meantime, the electrons were emitted from the substrates and were accelerated toward the plasma that induced a glow region in the vicinity of substrates (designated as 2nd glow in Fig. 1(a)).

The bias current is another effective parameter that can monitor the evolution of diamond nuclei in the BEN process. Figure 1(b) shows that the bias current increases monotonously with time when the diamond nuclei started to form on the Si substrates. The bias current reached a saturated value ($\sim$ 58 mA/cm^2) at around 7.5 min after the application of bias voltage, indicating that the diamond nuclei have fully covered the Si substrates. The inset in Fig. 1(b) shows the SEM micrograph of the Si substrates after BEN (−400 V) for 10.0 min, demonstrating that diamond clusters have been efficiently nucleated in this process. Notably, the conventional ultrasonication nucleation (UN) process usually required 45 min ultrasonication, followed by a 30 min MPE-CVD process to efficiently form the nucleation sites on Si substrates. The secondary glow discharge zone almost touches the substrate when

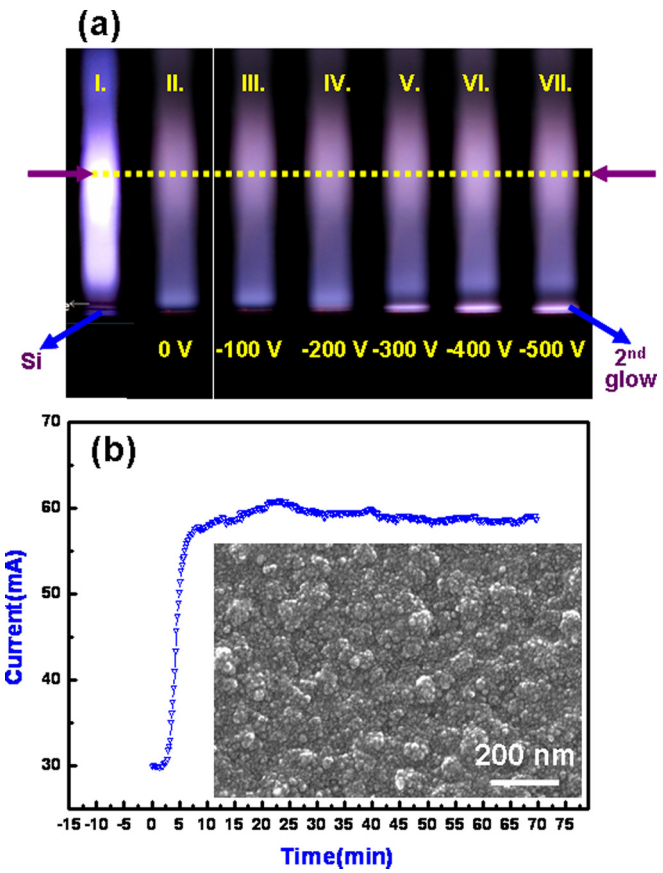

FIG. 1. (Color online) (a) The photographs of (I) the H_2 plasma and (II-VII) the CH_4 (9%) H_2 plasma used for synthesizing the diamond films under the BEG process, where the applied bias voltage is (I, II) 0 V, (III) −100 V, (IV) −200 V, (V) −300 V, (VI) −400 V, and (VII) −500 V; (b) the evolution of bias current with time in BEN process with the inset showing the SEM micrograph of the Si substrates, which were BEN for 10.0 min, showing the efficient formation of diamond nuclei.

the Si substrate is fully covered with the diamond nuclei in the BEN process (Fig. 1(a)). In contrast, the bare silicon substrates emit insignificant amount of electrons, resulting in very low bias current, and there is no secondary glow discharge induced.

The optical emission spectroscopy (OES) is a non-intruding method of monitoring the plasma that provides useful information for understanding the growth behavior of the diamond films in the CH_4/H_2 plasma. Figure 2(a) (spectrum I) shows that the CH_4/H_2 plasma used for growing diamond films contains a large proportion of atomic hydrogen, in accompaniment with some proportion of CH, C_2, and other hydrocarbon species.[25–27] The CH_3^+ species, which are presumed to be the diamond growing species, are non-emitting and cannot be monitored using OES. Application of bias voltage attracts the positively charged species, such as H^+, CH_3^+, CH^+ *et al.* and expels the electrons that markedly alter the plasma chemistry near the substrates. The nucleation and growth behavior for the diamond is, therefore, significantly enhanced, which will be discussed shortly. It should be noted that the diamond nuclei can be formed, fully covering the substrates, only when the CH_4/H_2 plasma contains a sufficient amount of CH_4, i.e., $CH_4 > 5\%$. When the CH_4 content in the CH_4/H_2 plasma is smaller than 5%, only discrete diamond particles are sparsely nucleated on the Si substrate, which is shown as the inset in Fig. 2(b).

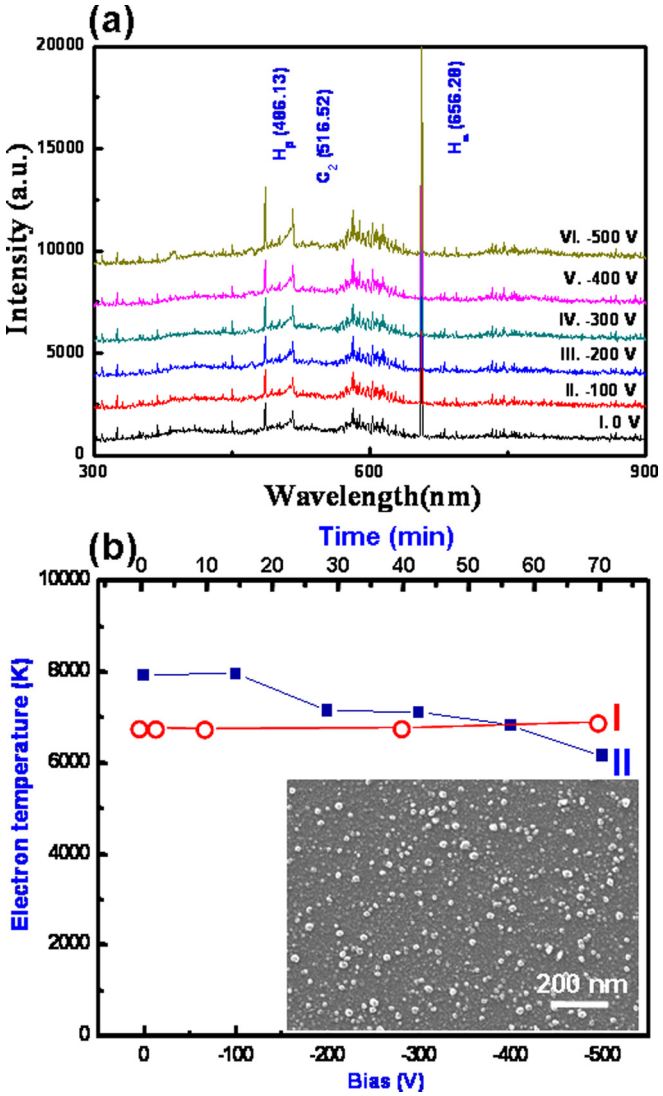

FIG. 2. (Color online) (a) The OES spectra for the CH_4/H_2 plasma under various applied voltage in the BEG process and (b) the corresponding electron temperature deduced from the OES spectra, using Boltzmann plot, where curve I is the T_e vs time (at −400 V) and curve II is the T_e vs bias voltage (at 30 min after the application of bias voltage). The inset shows the discrete diamond particulates, rather than complete diamond films, grown in $CH_4(5\%)/H_2$ plasma.

The plasma temperature (T_e) was estimated using the Boltzmann plot,[28,29] that was, using the formula

$$\frac{I_{ji}}{I_{kj}} = \frac{\lambda_{ki} A_{ji} g_j}{\lambda_{ji} A_{kj} g_k} \exp\left(\frac{E_k - E_j}{k_B T_{ex}}\right), \quad (1)$$

where I_{ji} and λ_{ji} are the intensity and wavelength of the spectral line corresponding to the transition between the E_j and E_i energy level, k_B is the Boltzmann constant, and A_{ji} and g_j are, respectively, the corresponding Einstein transition probability and statistical weight, which can be acquired from the literature.[30] The plasma temperature (T_e), corresponding to spectrum I in Fig. 2(a), is estimated to be around 6800 K, which insignificantly changes with the growth time (curve I, Fig. 2(b)), indicating that the plasma used for growing the diamond films is very stable.

Once the diamond nuclei were uniformly formed on the Si substrates, the diamond films can be grown on top of the nucleation layer using the same CH_4/H_2 plasma, no matter whether the bias voltage was applied or not in the growth period. In this study, the bias voltage in the BEG period was systematically changed for the purpose of investigating the effect of bias voltage on the granular structure of the diamond films. The Si substrates were first nucleated by BEN process under −400 V bias for 10 min to ensure the full coverage of the diamond nuclei, which was monitored by the saturation of the bias current, (stage I, Fig. 3(a)). The bias voltage was then switched to 0 to −500 V in the BEG period, which was also monitored by the evolution in the bias current (stage II, Fig. 3(a)). The saturated bias current in the BEG period was proportional to the bias voltage applied (Fig. 3(b)). The bias current in the BEG period was very stable, except for the case when −500 V was applied to the substrates. In the latter case, the resulting films possessed deteriorated microstructure and markedly degraded EFE, which will be shown shortly.

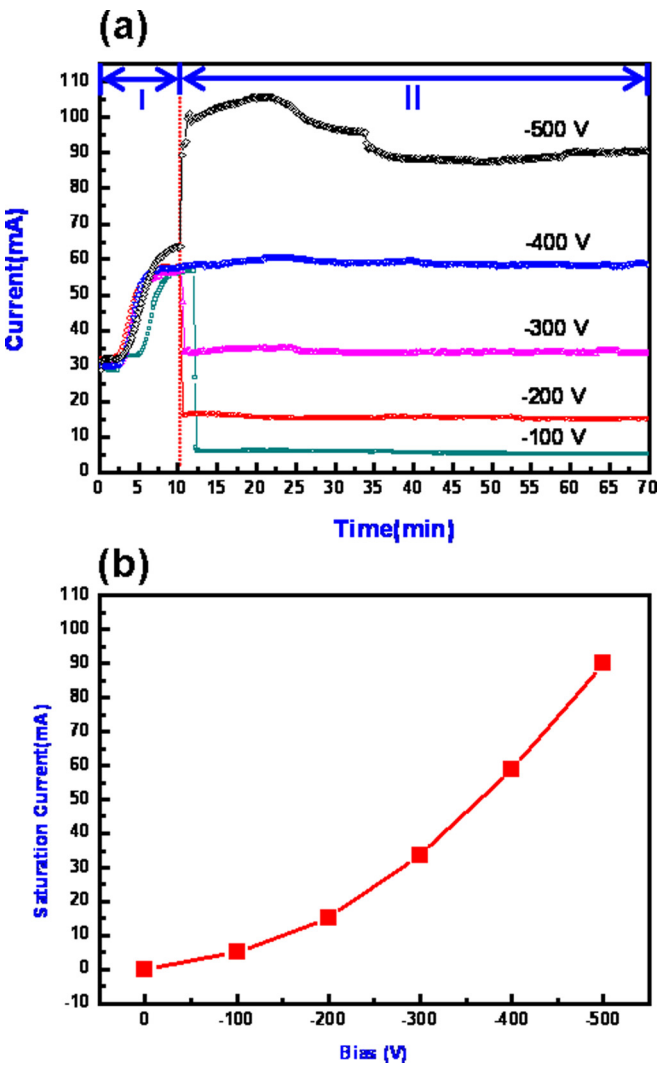

FIG. 3. (Color online) The evolution of bias current after application of −400 V bias voltage in BEN stage (stage I) and −100 to −500 V in BEG stage (stage II); (b) the variation of the saturated bias current vs bias voltage derived in (a).

The plasma under the application of negative bias voltage to the Si substrates was again monitored by the OES. Figure 2(b) (spectra II-VI) shows that the OES was not markedly altered, due to the presence of bias voltage, even though the appearance of the plasma near the Si substrates was greatly altered (cf. photographs II-VII, Fig. 1(a)). These photographs imply that the secondary glow region was induced due to the application of bias voltage. The higher the applied negative voltage was, the brighter and the thicker the secondary glow region. The secondary glow is presumably induced by the impact ionization of the neutral species (mainly the atomic hydrogen) by the electrons emitted from the diamond coating on Si substrates. Application of large negative bias voltage allowed the electrons to gain sufficient energy that almost instantaneously ionized the neutral species in the plasma once they were emitted from the diamond films. Detailed analyses on the OES in Fig. 2(a) using Boltzmann plot (cf. Eq. (1)) indicate that the plasma temperature (T_e) decreases slightly with the bias voltage (curve II, Fig. 2(b)). It should be reminded that the OES was taken from the center of the plasma, as indicated by the dotted line in Fig. 1(a). The decrease in T_e value with applied bias voltage implies that the energetic species in the plasma were slightly depleted in the center of the plasma as they were attracted toward the substrates.

The SEM micrographs of the diamond films BEG grown for 60 min (after 10 min BEN) are shown in Fig. 4, indicating that the size of grains in these films is only a few tens of nanometers, which are markedly smaller than the gains size for the conventional diamond films grown in CH_4/H_2 plasma without the application of bias voltages.[31] The magnitude of the bias voltage in the BEG process only moderately alters the granular structure of the diamond films, except for the one grown under −500 V applied voltage. The granular structure is blurred when the bias voltage is smaller than −200 V (Figs. 4(a)–4(c)) and become sharply defined when the bias voltage is larger than −300 V (Figs. 4(d) and 4(e)). When the films are grown under too large applied bias (−500 V), the granular structure is seriously deteriorated. Hillocks of hundreds of nanometers were resulted (Fig. 4(f)).

Raman spectroscopy, shown in Fig. 5(a), indicates that the crystallinity of the diamond films changed with the bias voltage markedly. The Raman spectra for the films grown under a bias voltage of 0 to −200 V (curves I-III, Fig. 5(a)) contain a sharp D-band at 1332 cm^{-1}, which characterizes the large grain diamond materials. These spectra also contain diffuse Raman resonance peaks (D*-, G-, ν_1 -, and ν_3-bands) with very small intensity. The D*-band at 1350 cm^{-1} and G-band at 1580 cm^{-1} represent the disordered carbons and

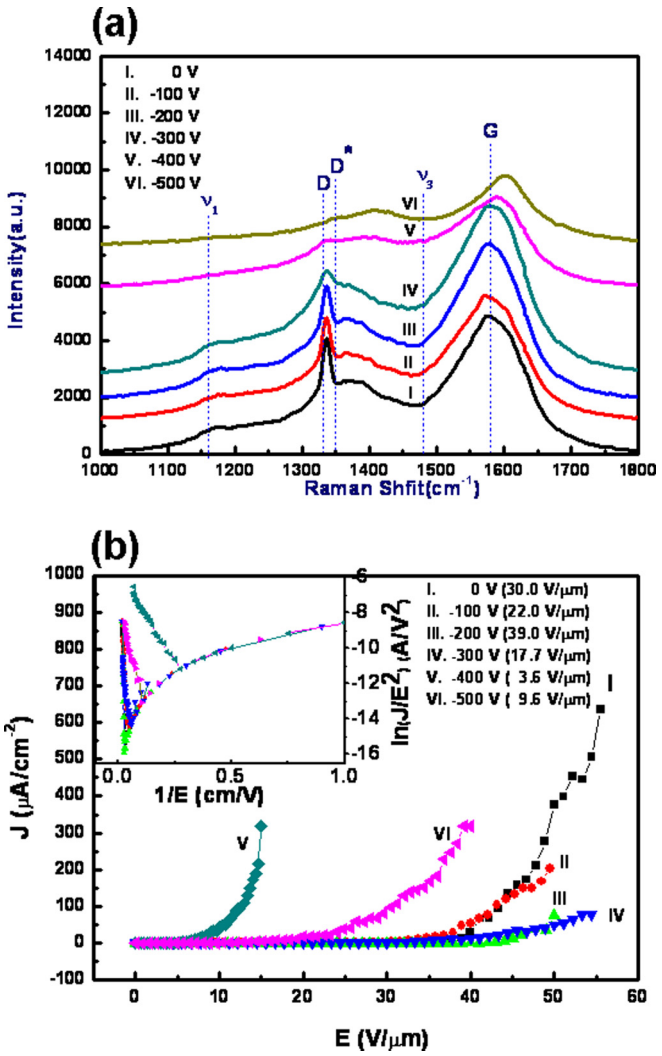

FIG. 5. (Color online) The (a) Raman spectroscopy and (b) EFE properties of BEN-BEG diamond films, which were BEG for 60 min after completion of 10 min BEN process, where the applied bias voltage is (I) 0 V, (II) −100 V, (III) −200 V, (IV) −300 V, (V) −400 V, and (VI) −500 V. The numbers shown in the parentheses in (b) are the turn-on field deduced from the corresponding F-N plots.

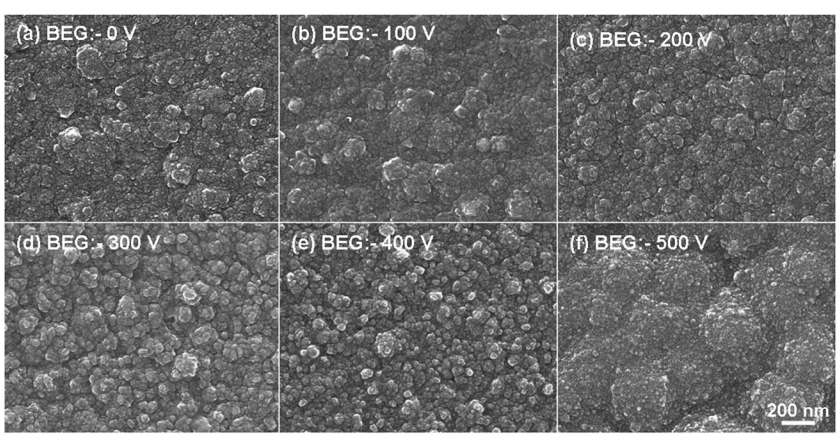

FIG. 4. SEM micrographs of BEN-BEG diamond films, which were BEG under (a) 0 V, (b) −100 V, (c) −200 V, (d) −300 V, (d) −400 V, and (f) −500 V for 60 min after completion of BEN process (10 min).

graphite,[32,33] whereas the ν_1-band at 1140 cm^{-1} and ν_3-band at 1480 cm^{-1} represent the trans-polyacetylene phase.[34,35] The diffuse Raman resonance peaks are characteristics of diamond film with ultra-small grains size.[36] These Raman spectra indicate that the BEG diamond films contain a small proportion of nano-sized diamond grains coexisting with the large diamond grains. The sharp D-band Raman resonance peak decreased markedly as the bias voltage increased larger than −300 V (curves IV−VI, Fig. 5(a)). The −400 V (−500 V) BEG diamond films contain only Raman resonance peaks with very broad resonance peaks. The sharp D-band resonance peak is no longer observable. Moreover, large negative bias voltage resulted in marked blue-shift of the G-band resonance peak toward 1600 cm^{-1} (curves V and VI, Fig. 5(a)), implying the induction of a large proportion of the graphitic phase. The significance of such a phenomenon will be further discussed shortly.

Figure 5(b) indicates that the EFE properties, the emission current density versus applied electric field (J-E) curves, of the BEG films is intimately correlated with their Raman characteristics. The inset in this figure shows the Fowler-Nordheim plot of the J-E curves, from which the turn-on field for triggering the EFE process was deduced. The EFE turn-on field (E_0) extracted from the J-E curves is listed in the inset of Fig. 5(b) (in parentheses). Figure 5(b) shows that the diamond films containing a sharp D-band Raman peak possess poor EFE properties with a large turn-on field ($E_0 > 17.7$ V/μm, curves I-IV), whereas the diamond films containing broad Raman peaks exhibit superior EFE properties with an E_0 smaller than 9.6 V/μm (curves V-VI). The BEG (−400 V)-grown diamond films exhibit the best EFE properties. The EFE process can be turned on at $E_0 = 3.6$ V/μm, and the EFE current density achieved 320 $\mu A/cm^2$ at an applied field of 15 V/μm. Such an EFE behavior is even better than those of the UNCD films grown in CH_4/Ar plasma.[16,17] The EFE properties are degraded for the BEG (−500 V, curve VI) films that, presumably, resulted from the deterioration of their granular structure.

B. Microstructural characteristics

The above-described results generate two unresolved questions concerning the role of negative bias voltage that are: (i) how does the BEG reduce the grain size? and (ii) how does it enhance the EFE properties of the diamond materials? To answer these questions, the detailed microstructure of the BEG films was examined using TEM. The interface between the diamond and Si substrate was investigated first to elucidate the nucleation process. Figure 6(a) shows a typical cross-sectional TEM micrograph of a region near the Si substrates for BEG films. The Si surface in contact with the diamond films is extremely rough, indicating that Si substrates were markedly damaged, due to the bombardment of the energetic species in the BEG process. To facilitate the comparison, the cross-sectional TEM micrograph of diamond films, which were pretreated by conventional ultrasonication nucleation (UN) process and were grown by the same MPE-CVD process without the bias voltage, is shown in Fig. 6(b). This figure reveals that, for the UN-derived diamond films, the Si surface in contact with the diamond is rather smooth. Figure 7 shows a more detailed microstructure investigated by high resolution TEM of the diamond-to-Si interfaces for the two diamond films. These micrographs indicate that the BEN-BEG process resulted in a subtly different nucleation mechanism from the UN process.[31,37] Figure 7(a) shows that, in the BEN process for forming diamond nuclei, the energetic carbonaceous species reacted with Si markedly, forming SiC particulates, as illustrated by the Fourier-transformed diffractogram (FT) corresponding to area 1 (FT_1). Diamond clusters are observable above the SiC particulate regions, which are indicated by area 2 and FT_2. In contrast, Fig. 7(b) shows that, although the UN process can also effectively induce the formation of diamond nuclei (area 3 and FT_3), a thin layer of amorphous carbon (a-C) layer around 2-3 nm in thickness (area 4, FT_4) always formed prior to the nucleation of diamond in the UN process.

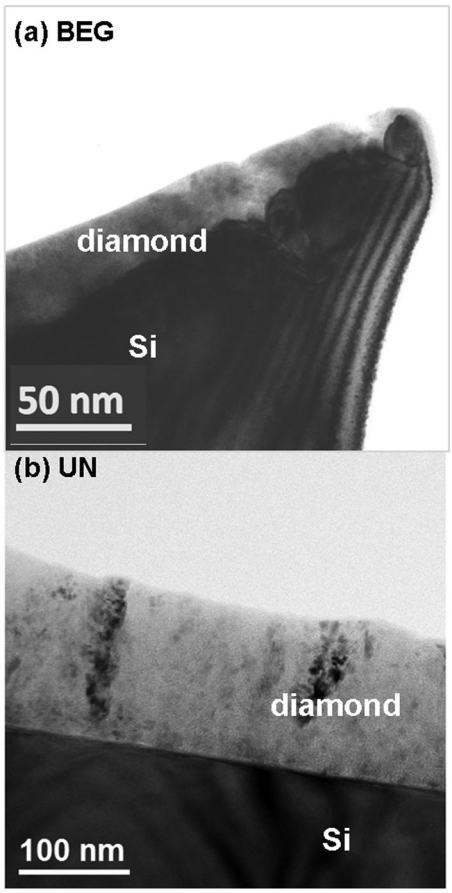

FIG. 6. The cross-sectional view of TEM bright field (BF) images of (a) the typical BEG (−400 V, 60 min)-grown diamond films and (b) the diamond films grown by the conventional MPE-CVD process after ultrasonication nucleation (UN) pretreatment.

The difference in the evolution of microstructure in the BEN and UN processes is more clearly illustrated by the composed dark field (c-DF) images, which are the superposition of the dark field images taken using diffraction spots, corresponding to the diamond, SiC, graphite (or amorphous phase), and Si phase. Figure 8(a) shows c-DF images corresponding to BEN films, illustrating that a large proportion of SiC particulates were induced, locating in between the diamond grains and the Si-substrates, whereas Fig. 8(b) reveals

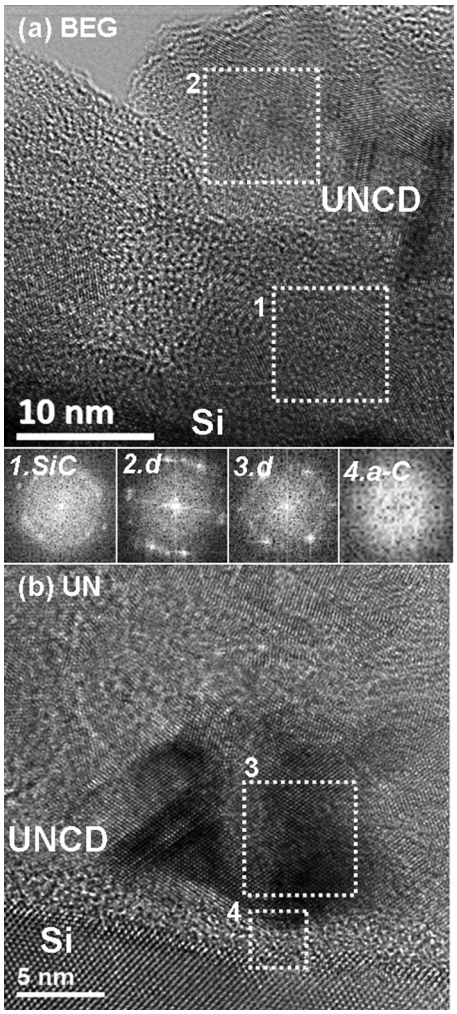

FIG. 7. The cross-sectional view of TEM structure images of the diamond in the vicinity of diamond-to-Si substrate for the films grown in (a) BEG process after 10 min BEN process and (b) conventional MPE-CVD process after ultrasonication nucleation pretreatment for 45 min. The insets show the FT images corresponding to the designated areas.

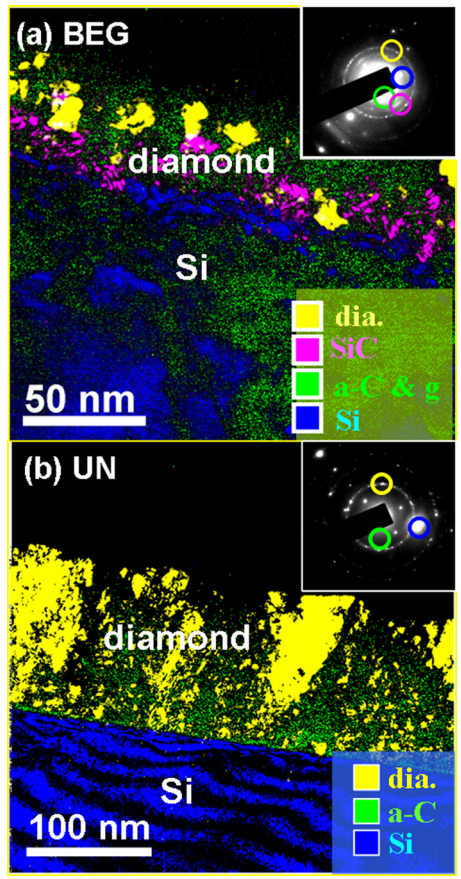

FIG. 8. (Color online) The composed dark field image (c-DF) of the region corresponding to Fig. 6, where the diamond films were grown by (a) the BEG (−400 V, 60 min) process and (b) the conventional MPE-CVD process after ultrasonication nucleation (UN) pretreatment. The c-DF images are the superposition of the dark field image taken from the diffraction spots corresponding to diamond, graphic, SiC, amorphous carbon, and Si.

that, in the UN process, a very thin layer of a-C phase (green color) was formed before the nucleation of diamond. Moreover, Fig. 8(a) shows that, in BEG films, the secondary nucleation process occurred frequently, such that the diamond particulates in BEG films remained at very small size (about tens of nano-meters). In contrast, Fig. 8(b) shows that, in the UN-derived films, the diamond grains grew continuously, resulting in columnar grains, and the size of the grains became larger as the grains grew.

To understand the role of applied negative bias voltage on modifying the EFE properties of the diamond films, the microstructure of the BEG (−100 V) and BEG (−400 V) diamond films were compared. Figure 9(a) shows the plane-view bright field (BF) TEM micrographs of the BEG (−100 V) diamond films. Ring-shaped selected area electron diffraction (SAED) patterns shown as the inset in Fig. 9(a) indicates that these films consist of randomly oriented diamond grains. Figure 9(b) shows the composed dark field (c-DF) TEM micrographs of these films, where the different color in c-DF corresponds to the dark field taken from different diffraction spots, i.e., they are different diamond grains. The c-DF image reveals that the grains in these diamond films are a few tens of nanometers in size, which is markedly smaller than the grains in diamond films grown by conventional MPE-CVD process without the application of bias voltage. Moreover, contrary to the sharp grain boundaries commonly observed for the conventional large grain granular structured diamond films, Fig. 9(a) shows that the grain boundaries of the BEG (−100 V) diamond films are diffused.

Figure 10(a) shows an enlarged TEM structure image of a typical diamond grain (region I, Fig. 9(a)), which is oriented in some zone axis, indicating that the grains contain a large proportion of planar defects. There are regions containing parallel fringes with irregular spacing (area I, Fig. 10(a)), which corresponds to stacking fault[38] (implied by the streaks in FT_I), and regions containing parallel fringes with regular spacing (area II, Fig. 10(a)), which corresponds to hexagonal diamond[38] (implied by the systematic rows of diffraction spots in FT_{II}). The complicated microstructure is the typical characteristic of the grains in these diamond films. Such a complicated granular structure is very alike with that of the large aggregate induced in ultra-nanocrystalline diamond (UNCD) films when some proportion of H_2 species were incorporated in CH_4/Ar plasma.[39] However, for the films grown in H_2-incorporated CH_4/Ar plasma (without the bias

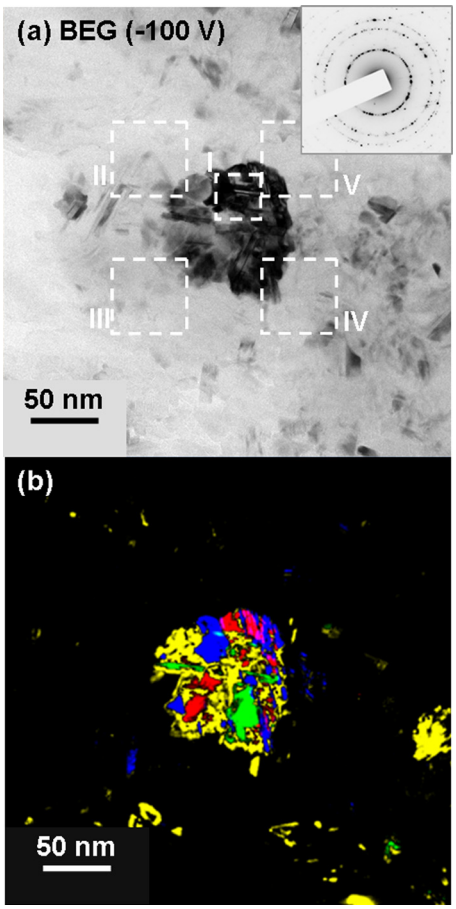

FIG. 9. (Color online) The (a) bright field (BF) and (b) composed dark field (c-DF) images of the BEG (–100 V, 60 min)-grown diamond films after 10 min BEN process.

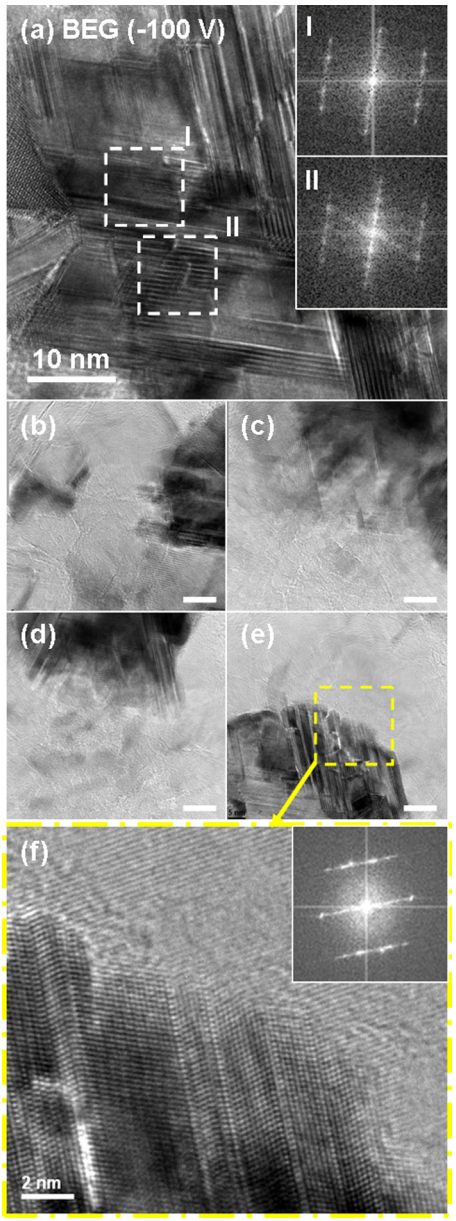

FIG. 10. (Color online) (a) The TEM structure image of the region I in Fig. 9, showing the presence of planar defects; (b) to (e) the TEM structure image of the regions II to V in Fig. 9, respectively, showing the microstructure of grain boundary regions; (f) the enlarged TEM structure image of the region designated in (e).

voltage), the large aggregates were only sparsely distributed among the matrix of nano-diamond grain (~5 nm in size) matrix. In contrast, for the BEG (−100 V) diamond films, the diamond grains about a few tens of nanometers were uniformly distributed over the samples. The presence of planar defects in diamond grains implies that the grain grew in a very rapid rate in the BEG process.

The diffused grain boundaries for these films were detailedly examined. Figures 10(b) to 10(e) show the detailed microstructure of the regions II to V designated in Fig. 9(a), respectively, which are the regions adjacent to region I. It should be noted that these circumferential regions are also diamond grains, but are oriented in a non-diffracting direction. These figures show that the lattice fringes were smeared out gradually from the crystalline region (region I) toward the adjacent regions. There are no clear boundaries between them. Such a phenomenon is more clearly illustrated in Fig. 10(f) for the enlarged TEM structure image of the region designated in Fig. 10(e), implying that the diamond transformed gradually from the crystalline structure toward the amorphous one at grain boundaries without a sharp transition boundary.

High CH_4 concentration contained in the CH_4/H_2 plasma could be one of the factor that reduces the grain size for the BEG diamond films.[37] However, it is believed that the more important cause, resulting in nano-diamond granular structure for these films, is the application of large bias voltage in the BEG process. Under the application of large bias voltage, all the positively charged species (H^+, CH^+, CH^{3+}, C_2^+,…) gained large kinetic energy and were accelerated toward the Si substrates. On one hand, the energetic atomic hydrogen can etch more efficiently the amorphous carbons (or carbonaceous species) adhered on the diamond nuclei that favors the enlargement of the diamond grains.[39] On the other hand, the energetic carbonaceous and hydrocarbon species may increase the rate of accumulation of the carbonaceous species on the diamond surface, inducing the secondary nucleation process. Presumably, the re-nucleation process is predominating in the BEG growth of the diamond films, as ultra-small grain microstructure are always observed for the BEG films.

In the conventional CH_4/H_2 MPE-CVD process (without the bias voltage), the CH_3 species are presumed to be the diamond-growing species. The abundant atomic hydrogen contained in the CH_4/H_2 plasma is known to efficiently etch the non-sp^3 bonds formed at the surface of diamond that favored the continuous growth of diamond grains. The diamond grains grew columnar-wisely, resulting in large-grain granular structure. The secondary nucleation process can be induced whenever the non-sp^3 bonds accumulated in a fast rate on the surface of diamond grains. The above-described nano-grain granular structure observed for the BEG (−100 V) diamond films implied that the negative bias increased markedly the adherence of the carbonaceous species (C_2 or CH), which are abundant in the CH_4/H_2 plasma, such that the carbonaceous species accumulated on the diamond surfaces faster than the etching of these species by the atomic hydrogen. The secondary nucleation process readily occurred from the carbonaceous layer. The TEM microstructural observations shown in Figs. 9 and 10 support the argument that, in the BEG process, energetic carbonaceous species were accumulated on the diamond grain surface that gradually deteriorate the crystallinity of the diamond lattice and, in the meantime, trigger the formation of new diamond nuclei, resulting in secondary diamond grains.

A similar formation mechanism can also account for the obtained granular structure for the diamond films grown with −400 V bias voltage, but still cannot explain how the larger bias voltage results in marked improvement in EFE properties. For the purpose of elucidating the authentic factor that enhanced the EFE properties of these films, the detailed microstructure of the BEG (−400 V) diamond films was also examined. Figure 11(a) shows the plane-view TEM micrograph of BEG (−400 V) diamond films, indicating again that the BEG (−400 V) films also contain randomly oriented diamond grains, which is also implied by the ring-shaped SAED pattern shown as the inset in this figure. The grains' size distribution is, again, illustrated by the composted dark field (c-DF) image shown in Fig. 11(b), which reveals that the BEG (−400 V) films contain even smaller diamond grains, as compared with those in BEG (−100 V) diamond films (cf. Figure 9). Figure 12(a) shows the TEM structure image of a region oriented near some zone axis (region I, Fig. 11(a)). The diamond grain is essentially defectless in the interior of the grain (area 1, FT_1), but contains a large proportion of planar defects near the grain boundaries (area 2, FT_2). Again, Fig. 12 indicates that there is no clear boundaries between the adjacent grains, implying that there exists an amorphous phase in the grains boundaries of these films. The grain boundary phase surrounding the diamond grains is too faint, in contrast, to be clearly resolvable, due to strong contrast of the diamond grains. To clearly resolve the existence of the grain boundary phases, the diamond grains, which are away from a zone axis, diffracting no electrons, were examined. Figures 12(b) to 12(e) show the TEM structure images of the regions, which are in adjacent to the region I in Fig. 11(a) (regions II to V, respectively, in Fig. 11(a)). These regions diffract insignificantly the electrons, showing no contrast, that render the detail microstructure of the background phase observable. In these figures,

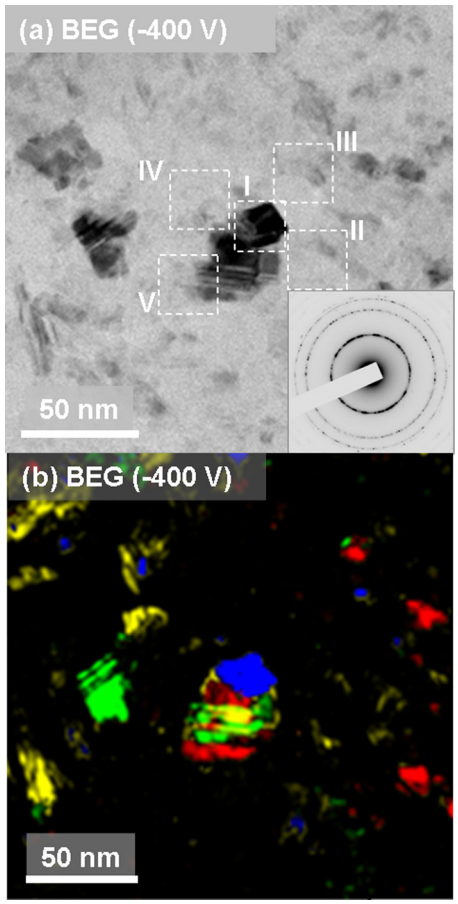

FIG. 11. (Color online) The (a) bright field (BF) and (b) composed dark field (c-DF) images of the BEG (−400 V, 60 min)-grown diamond films after 10 min BEN process.

regions of curved fringes are observable. The corresponding Fourier-transformed (FT) diffractograms shown as insets in these figures (FT_3 to FT_6) indicate that these curved fringes are a-few-layer graphite. Notably, in the junction of 3 grain boundaries, the graphitic phase is in a form of vortexes (highlighted by arrows in Figs. 12(b)–12(e)). The vortexes are presumably the end view of the graphitic filaments, which will be further illustrated shortly.

The cross-sectional microstructure of the region near the diamond-to-Si interface for the BEG (−400 V) films was examined in detail. Figure 13(a) shows a diamond grain nucleated near this region. This grain contains twins with 111 twin plane, which is more clearly illustrated by the FT image (inset 1, Fig. 13(a)). The detail analysis on the FT_1 image is schematically illustrated in inset 2, where the main spots corresponding to the original crystal are shown as solid circles and those corresponding to twin are shown as dotted circles (the corresponding Mille index is indicated with a subscription "t"). However, this diamond grain (~10 nm in size) is essentially defectless as compared with the diamond grains in BEG (−100 V) films (cf. Figure 10(a)). This figure reveals that a secondary nucleation process occurred frequently, even in the region near the diamond-to-Si interface, such that the diamond grains do not have a chance to grow larger. Figure 13(b) shows the structure images near the diamond-to-Si interface. These figures indicate that, besides the presence of SiC

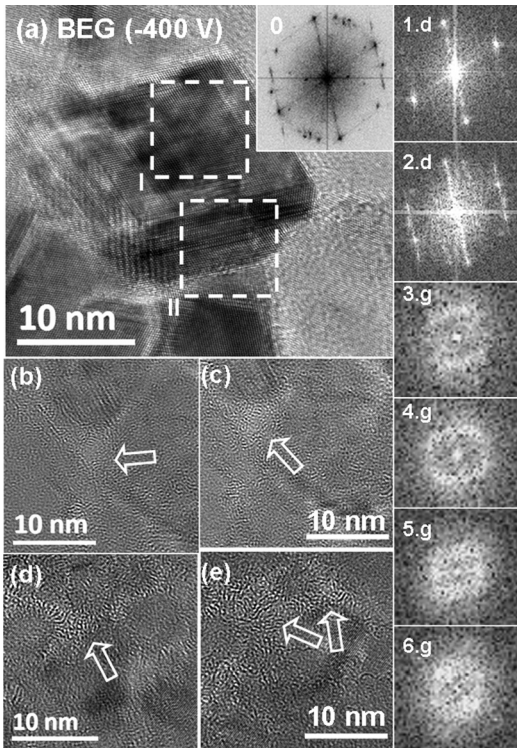

FIG. 12. (a) The TEM structure image of the region I in Fig. 11 showing the presence of planar defects, with the insets 1 and 2 showing the FT images corresponding to region I and II; (b) to (e) the TEM structure image of the regions II to V in Fig. 11, respectively, showing the microstructure of grain boundary regions. The insets 3 to 6 show the FT images corresponding to (b) to (e).

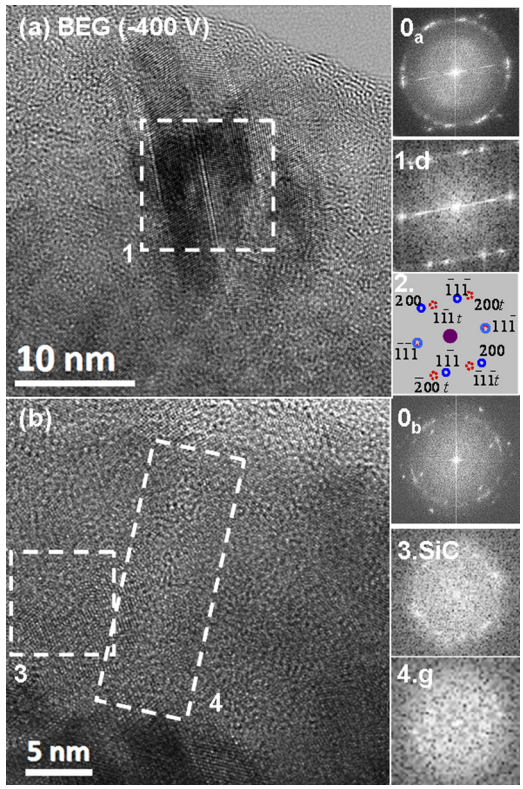

FIG. 13. (Color online) The cross-sectional TEM structure images of the diamond in the vicinity of Si substrate for the films grown in BEG (−400 V) process after 10 min BEN process: (a) the diamond grains formed at a distance from the diamond-to-Si interfacial region and (b) the SiC clusters and nano-graphitic phase formed at the interface.

clusters (area 3, FT_3) formed prior to the nucleation of diamond, there exists an a-few-layer graphitic phase stemming from the interface region upward (area 4, FT_4).

Notably, only the application of negative bias voltage can induce the formation of nano-grain granular structure for the diamond films. Application of positive bias voltage enhanced the (100) preferred oriented grains and the growth rate for the diamond films, but will not decrease the grains size.[40] Such a phenomenon supports the above-described arguments for the formation mechanism of the nano-grain granular structure under the effect of negative bias voltage. The above-described observations reveal that the application of −100 V bias voltages is sufficient for inducing the secondary nucleation process, resulting in nano-grain granular structure for the diamond films. However, the EFE behavior for the BEG films can be markedly enhanced only when large (−400 V) bias voltage was applied such that the crystalline nano-graphite clusters were induced, especially when the nano-graphite clusters were interconnected, forming a graphite filament. The presence of graphitic filaments observed in Fig. 13(b) is in accord with the vortexes observed in Figs. 12(b)–12(e). Apparently, only when the positively charged carbonaceous species (C_2^+. CH^+, CH_3^+,…) possess large enough kinetic energy (e.g., −400 eV) can they induce the transformation of accumulated amorphous carbon into nano-graphite. The carbonaceous species with insufficient kinetic energy (e.g., −100 eV) can only deteriorate the crystalline diamond lattice and induce the re-nucleation process, but cannot convert the amorphous carbon into crystalline nano-graphite. Only amorphous carbon resulted. Restated, the authentic factor that large negative bias voltage (−400 V) enhanced the EFE properties of the diamond films, in addition to the reduction on the grain size of the diamond films, is the induction of the nano-graphitic filaments, stemming all the way from the diamond-to-Si interfaces toward the surface of the diamond films.

IV. CONCLUSION

The evolution of plasma and the characteristics of the diamond films, including SEM morphology, Raman spectroscopy, and EFE properties, in the BEN-BEG process were systematically investigated. TEM examinations indicate that, in the BEG process, the carbonaceous species reacted with Si, forming SiC particulates, which then nucleated the diamond clusters. Such a process is markedly different from the nucleation mechanism in the ultrasonication nucleation process, in which an amorphous carbon layer was formed prior to the nucleation of diamond. While the BEN process can efficiently form diamond nuclei on the Si-substrates, the BEG for large enough applied field (>−400 V) and sufficient long period (>60 min) is needed to develop the diamond films with proper microstructure that exhibit good EFE properties. Moreover, BEG under −100 V bias voltages already increased the accumulation rate of carbonaceous species on diamond, inducing the secondary nucleation process and resulting in nano-diamond granular structure. However, only

when BEG is under −400 V can the nano-graphitic filaments be formed in addition to induction of the re-nucleation process. The EFE process for the films' BEN for 10 min in an applied field of −400 V followed by the BEG under −400 V for 60 min can be turned on at a field as small as 3.6 V/μm, attaining a EFE current density as large as 325 μA/cm^2 at an applied field of 15 V/μm. Such an EFE behavior is even superior to that of the UNCD films grown in CH_4/Ar plasma. The smallness in diamond grains seems not to be the main cause of the enhanced EFE properties. The prime factor that improved the EFE properties of the BEN-BEG diamond films is the induction of the nano-graphitic filaments along the thickness of the films that facilitate the transport of electrons through the films.

ACKNOWLEDGMENTS

The authors would like to thank the financial support of the National Science Council, R. O. C. through the project NSC99-2119-M-032-003-MY2.

[1]J. E. Field, *The Properties of Diamonds* (Academic, London, 1979).
[2]H. Liu and D. S. Dandy, Diamond Relat. Mater. **4**, 1173 (1995).
[3]J. C. Angus, H. A. Will, and W. S. Stanko, J. Appl. Phys. **39**, 2915 (1968).
[4]B. V. Spitsyn, L. L. Bouilov, and B. V. Derjaguin, J. Cryst. Growth **52**, 219 (1981).
[5]J. van der Weide, Z. Zhang, P. K. Baumann, M. G. Wensell, J. Bernholc, and R. J. Nemanich, Phys. Rev. B **50**, 5803 (1994).
[6]M. W. Geis, N. N. Efremow, J. D. Woodhouse, M. D. Mcaleese, M. Marchywka, D. G. Socker, and J. F. Hochedez, IEEE Electron Device Lett. **12**, 456 (1991).
[7]W. P. Kang, J. L. Davidson, A. Wisitsora-at, D. V. Kerns, and S. Kerns, J. Vac. Sci. Technol. B **19**, 936 (2001).
[8]A. T. Sowers, B. L. Ward, S. L. English, and R. J. Nemanich, J. Appl. Phys. **86**, 3973 (1999).
[9]P. T. Joseph, N. H. Tai, H. Niu, U. A. Palnitkar, W. F. Pong, H. F. Cheng, and I. N. Lin, Diamond Relat. Mater. **17**, 1812 (2008).
[10]Y. C. Lee, S. J. Lin, I. N. Lin, and H. F. Cheng, J. Appl. Phys. **97**, 054310 (2005).
[11]C. F. Shih, K. S. Liu, and I. N. Lin, Diamond Relat. Mater. **9**, 1591 (2000).
[12]Y. H. Chen, C. T. Hu, and I. N. Lin, Appl. Phys. Lett. **75**, 2857 (1999).
[13]R. G. Farrer, Solid State Commun. **7**, 685 (1969).
[14]R. G. Farrer and L. A. Vermeulen, J. Phys. C **5**, 2762 (1972).
[15]T. D. Corrigan, A. R. Krauss, D. M. Gruen, O. Auciello, and R. P. H. Chang, Mater. Res. Soc. Symp. Proc. **593**, 233 (2000).
[16]D. Zhou, A. R. Krauss, L. C. Qin, T. G. McCauley, D. M. Gruen, T. D. Corrigan, R. P. H. Chang, and H. Gnaser, J. Appl. Phys. **82**(9), 4546 (1997).
[17]A. R. Krauss, D. M. Gruen, D. Zhou, T. G. McCauley, L. C. Qin, T. D. Corrigan, O. Auciello, and R. P. H. Chang, Mater. Res. Soc. Symp. Proc. **495**, 299 (1998).
[18]D. C. Li, L. Dai, S. Huang, A. W. H. Mau, and Z. L. Wang, Chem. Phys. Lett. **316**, 349 (2000).
[19]E. F. Kukovitsky, S. G. L'vov, and N. A. Sainov, Chem. Phys. Lett. **317**, 65 (2000).
[20]S. B. Sinnott, R. Andrews, D. Qian, A. M. Rao, Z. Mao, E. C. Dickey, and F. Derbyshire, Chem. Phys. Lett. **315**, 25 (1999).
[21]G. Eda, H. Emrah Unalan, N. Rupesinghe, G. A. J. Amaratunga, and M. Chhowalla, Appl. Phys. Lett. **93**, 233502 (2008).
[22]Z. S. Wu, S. Pei, W. Ren, D. Tang, L. Gao, B. Liu, F. Li, C. Liu, and H. M. Cheng, Adv. Mater. **21**, 1756 (2009).
[23]X. Y. Zhong, Y. C. Chen, N. H. Tai, I. N. Lin, J. M. Hiller, and O. Auciello, J. Appl. Phys. **105**(3), 034311 (2009).
[24]R. H. Fowler and L. Nordheim, Proc. R. Soc. London, Ser. A **119**, 173 (1928).
[25]D. Zhou, T. G. McCauley, L. C. Qin, A. R. Krauss, and D. M. Gruen, J. Appl. Phys. **83**, 540 (1998).
[26]P. W. May, Yu. A. Mankelevich, J. N. Harvey, and J. A. Smith, J. Appl. Phys. **99**, 104907 (2006).
[27]J. R. Rabeau, P. John, J. I. B. Wilson, and Y. Fan, J. Appl. Phys. **96**, 6724 (2004).
[28]M. L. Brake, and T. E. Repetto, IEEE Trans. Plasma Sci. **17**(1), 60 (1989).
[29]Y. Kaga, S. Tsuge, K. Kitagawa, and N. Arai, Microchem. J. **63**, 34 (1999).
[30]See http://physics.nist.gov/asd3 for information about the NIST Atomic Spectra Database (version 3.1.2).
[31]C. S. Wang., H. C. Chen, W. C. Shih, H. F. Cheng, and I. N. Lin, Diamond Relat. Mater. **19**, 138 (2010).
[32]J. Michler, Y. Von Kaenel, J. Stiegler, and E. Blank, J. Appl. Phys. **81**(1), 187 (1998).
[33]A. C. Ferrari and J. Robertson, Phys. Rev. B **61**, 14095 (2000).
[34]Z. Sun, J. R. Shi, B. K. Tay, and S. P. Lau, Diamond Relat. Mater. **9**, 1979 (2000).
[35]A. C. Ferrari and J. Robertson, Phys. Rev. B **63**, 121405 (2001).
[36]D. Zhou, T. G. McCauley, L. C. Qin, A. R. Krauss, and D. M. Gruen, J. Appl. Phys. **83**(1), 540 (1998).
[37]D. Pradhan and I. N. Lin, ACS Appl. Mater. Interface **1**(7), 1444 (2009).
[38]I. N. Lin, H. C. Chen, C. S. Wang, Y. R. Lee, and C. Y. Lee, Cryst. Eng. Comm. **13**, 6082 (2011).
[39]C. S. Wang, H. C. Chen, H. F. Cheng, and I. N. Lin, J. Appl. Phys. **107**, 034304 (2010).
[40]D. Saito, H. Isshiki, and T. Kimura, Diamond Relat. Mater. **18**, 56 (2009).